

Mixing and segregation of ring polymers: spatial confinement and molecular crowding effects

This content has been downloaded from IOPscience. Please scroll down to see the full text.

2014 New J. Phys. 16 053047

(<http://iopscience.iop.org/1367-2630/16/5/053047>)

View [the table of contents for this issue](#), or go to the [journal homepage](#) for more

Download details:

This content was downloaded by: metzler

IP Address: 217.41.236.77

This content was downloaded on 25/05/2014 at 15:30

Please note that [terms and conditions apply](#).

Mixing and segregation of ring polymers: spatial confinement and molecular crowding effects

Jaehoh Shin¹, Andrey G Cherstvy¹ and Ralf Metzler^{1,2}

¹Institute for Physics & Astronomy, University of Potsdam, 14476 Potsdam-Golm, Germany

²Department of Physics, Tampere University of Technology, 33101 Tampere, Finland

E-mail: rmetzler@uni-potsdam.de

Received 7 January 2014, revised 26 March 2014

Accepted for publication 14 April 2014

Published 23 May 2014

New Journal of Physics **16** (2014) 053047


doi:[10.1088/1367-2630/16/5/053047](https://doi.org/10.1088/1367-2630/16/5/053047)

Abstract

During the life cycle of bacterial cells the non-mixing of the two ring-shaped daughter genomes is an important prerequisite for the cell division process. Mimicking the environments inside highly crowded biological cells, we study the dynamics and statistical behavior of two flexible ring polymers in the presence of cylindrical confinement and crowding molecules. From extensive computer simulations we determine the degree of ring-ring overlap and the number of inter-monomer contacts for varying volume fractions ϕ of crowders. We also examine the entropic demixing of polymer rings in the presence of mobile crowders and determine the characteristic times of the internal polymer dynamics. Effects of the ring length on ring-ring overlap are also analyzed. In particular, on systematic variation of the fraction of crowding molecules, a $(1 - \phi)$ -scaling is found for the ring-ring overlap length along the cylinder axis, and a non-monotonic dependence of the 3D ring-ring contact number with a maximum at $\phi \approx 0.2$ is obtained. Our results demonstrate that polymer rings are demixed and separated by particular entropy-favourable partitioning of crowders along the axis of the cylindrical simulation box. These findings help to rationalize the implications of macromolecular crowding for circular DNA molecules in confined spaces inside bacteria as well as in localized cellular compartments inside eukaryotic cells.



Content from this work may be used under the terms of the [Creative Commons Attribution 3.0 licence](https://creativecommons.org/licenses/by/3.0/). Any further distribution of this work must maintain attribution to the author(s) and the title of the work, journal citation and DOI.

 Online supplementary data available from stacks.iop.org/njp/16/053047/mmedia

Keywords: polymers, confinement, crowding

1. Introduction

The statistical effects of spatial external confinement on the properties of ring polymers such as those depicted in figure 1 is important to the physical understanding of the entropy-driven segregation of the two bacterial daughter chromosomes upon cell division [1] and the structure of eukaryotic metaphase chromosomes [2–4]. For rod-like bacteria cells such as *E. coli*, *Bacillus subtilis*, or *streptobacillus* a directed motion and segregation of duplicated chromosomes along the cell axis is detected after DNA replication; see, for instance, [5]. In eukaryotes, upon decondensation of the chromosomes in a strongly limited space inside the nucleus, the existence of chromosomal territories [6, 7] indicates an ultra-slow polymer mixing dynamics [8–11]. Knotting of DNA molecules in tight spaces inside viral capsids is yet another example of the effects of external polymer confinement in biology [12–15]. *In vitro*, the elongation and compaction of long DNA molecules confined in nano-channels upon increasing fraction of the crowding agent was indeed detected [16].

Internal polymer confinement *in vivo* is due to macromolecular crowding, which enforces DNA condensation in bacterial cells [17, 18] where the volume fraction occupied by crowding macromolecules such as RNA, ribosomes, or other biomacromolecules reaches $\phi = 30 \dots 35\%$ [19–22]. The abundance of crowding agents effects a viscoelastic environment [23–25] that severely alters the diffusional dynamics of submicron endogenous cytoplasmic granules and of tracers inside living cells [26–31]. Concurrently the internal dynamics of polymers and the macromolecular association kinetics inside biological cells are dramatically changed [32–34]. The effect of various polymeric crowders on the opening-closing dynamics of DNA hairpins was recently experimentally probed in [35]. Crowding can also facilitate phase separation and compartmentalization of the bacterial cytoplasm. In theoretical models, inert spherical obstacles are often used to mimic highly crowded interiors of bacterial [19] and eukaryotic [36] cells. Crowding particles cause effective interactions between the polymer segments of the same chain and between the two chains in confinement, as studied in the present paper. From a theoretical perspective, overlapped segments of long polymer chains experience entropic repulsion scaling with the number of overlapping polymer blobs [37]. In a dense polymer melt the entanglements of the chains also slow down the polymer dynamics [38, 39]. In the presence of static obstacles, the extension and dynamics of ring polymers on a lattice was analyzed in [40].

A number of simulation studies of polymers under external confinement in various geometries have appeared in the literature in recent years [41–51]. In particular, the size scaling of ring polymers in dense melts was analyzed by computer simulations in [47]. As the concentration of rings c grows and the effective volume available for their expansion decreases, the scaling exponent for the radius of gyration $\langle R_g^2 \rangle \simeq n^{2\nu}$ decreases from $\nu = 3/5$ to $\nu \approx 0.3$, mirroring impeded polymer extension. Neighboring rings in dense melts thus induce a spherical caging effect, and their dimension was shown to scale as $\langle R_g^2 \rangle \sim c^{-0.59}$ in terms of the ring

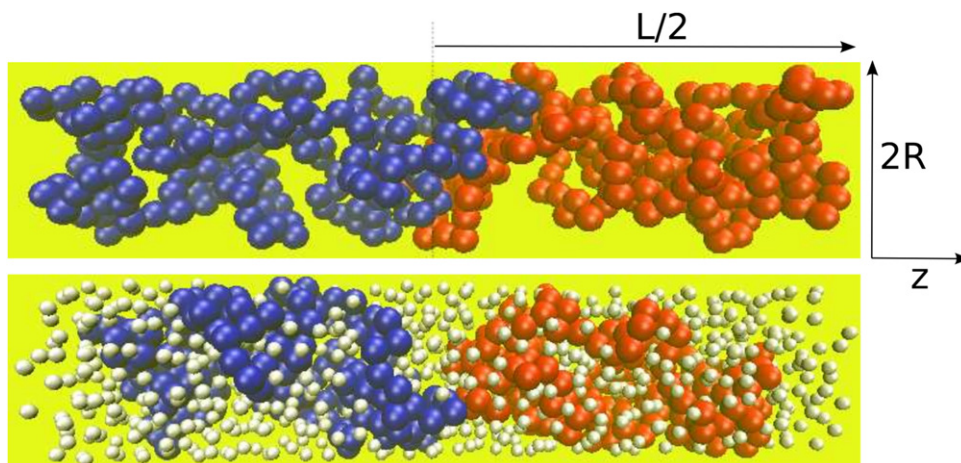


Figure 1. Typical conformations of two polymer rings (rendered in red and blue, respectively) in a cylindrical confinement. Parameters: the rings are $n = 200$ monomers long; the cylinder radius is $R = 4.5\sigma$ in terms of the monomer size σ , with the fraction of crowders $\phi = 0$ (top) and $\phi = 0.182$ (bottom). Crowding particles, which are equal in size to the chain monomers, are shown in this image in light yellow with $1/2$ of their actual radius, to improve the visibility of the image. Although the cylinder radius in the majority of our computations is much smaller than the size of a typical bacteria, $L = 35\sigma$, we prove below that the results for the inter-chain crossing probability are scalable to bigger bacterial-sized systems.

concentration [47]. The segregation of semi-flexible macromolecules in nano-channels was shown theoretically in [52]. Ring polymers in confinement were successfully used to model the bacterial chromosome [44] and to rationalize the implications of supercoiling for the contact maps of eukaryotic interphase chromosomes [45]. More bio-related experimental examples of polymer rings in confinement can be found in [7, 38, 44, 53]. For more experimental observations of confined polymers, including DNAs in nano-channels and chromatin folding, see [54, 55].

More specific with respect to our present study, the entanglement propensity of ring and linear polymers under external cylindrical confinement and the consequences for the phenomenon of DNA homologous recombination were analyzed recently in [53]. It was shown that linear chains penetrate into one another significantly more easily than ring polymers. Finally, the threading of ring polymers inside a polymer gel was recently studied by simulations [56].

The statistical properties of linear and ring polymers in the presence of crowding effects were considered in a number of theoretical and simulations studies. In particular, the behavior of single knotted polymer rings on a regular lattice of obstacles was simulated in [57].³ For random-loop and self-avoiding polymers in the presence of crowding, the computer modelling

³ Two scaling regimes for ring dimensions were predicted in [57]. Namely, rings smaller than the lattice size b behave as a self-avoiding walk, $\langle R_g^2 \rangle \sim n^{1.15}$, while large rings follow the law for branched polymers [58]: $\langle R_g^2 \rangle \sim n^1$. Similarly, for knotted rings the dynamics turns from a self-avoiding walk to a branched polymer dynamics [57].

in [59, 60] demonstrated a non-monotonic dependence of $\langle R_g^2 \rangle$ on the volume fraction occupied by the crowders, ϕ , featuring a slight minimum in the chain dimensions at $\phi \approx 0.2$. Related to this, the rates of chemical diffusion-limited reactions in molecularly crowded media in confined environments was shown to reveal a maximum at $\phi \approx 0.2$ [61].

In a biophysical context, the effect of crowding on gene regulation was studied with respect to facilitated diffusion and target search on DNA by DNA-binding proteins in [34, 62]. The translocation of polymers between the two reservoirs with crowders of equal [63] and non-equal [64] sizes was rationalized by simulations. The implications of crowding environments inside nano-channels were recently examined by simulations [65]. Finally, the effects of crowders on the looping probabilities of polymer chains in the presence of external confinement and molecular crowding is also important [66].

Below, we take a step further and analyze the joint effect of external confinement and internal crowding for two unknotted ring polymers in a model rod-shaped bacteria cell. More concretely, we perform molecular dynamics simulations for two polymer rings confined in a cylindrical volume in the presence of mobile crowders, which are subject to the same thermal bath, as illustrated in figure 1. We analyze how the entropic repulsion of these thermally agitated ring polymers becomes altered under these crowding conditions.

The paper is organized as follows. In the next section, we present the details of the simulations model. In section 3 we rationalize the effects of external cylindrical confinement and internal confinement by the crowding obstacles. The main results for the static properties of the mutual overlap of the polymer rings and their dynamic characteristics are presented. In section 4 we discuss the basic results and their implications for the biological system and with respect to polymer physics.

2. Model and implementation of the simulations

2.1. Polymer chains

The standard finitely extensible non-linear elastic (FENE) potential is used to model the interactions between the monomers in our polymer chains in the bead-spring coarse-grained model of the DNA molecule, namely,

$$U_{\text{FENE}}(r) = -\frac{k}{2} r_{\text{max}}^2 \ln \left(1 - \frac{r^2}{r_{\text{max}}^2} \right). \quad (1)$$

Here k is the spring constant acting between nearest-neighbor beads and r_{max} is the maximum allowed separation between neighboring monomers. The total number of monomers in the ring polymers varies in the simulations in the range $n = 60 \dots 350$. Excluded-volume interactions between the polymer segments are introduced by the truncated Lennard-Jones repulsion (Weeks-Chandler-Andersen potential), that is,

$$U_{\text{LJ}}(r) = \begin{cases} 4\epsilon \left[\left(\frac{\sigma}{r}\right)^{12} - \left(\frac{\sigma}{r}\right)^6 \right] + \epsilon, & r < 2^{1/6}\sigma \\ 0, & \text{otherwise.} \end{cases} \quad (2)$$

We here introduced the monomer-monomer distance r ; σ is the monomer diameter and ϵ is the strength of the potential. We set $k = 30$, $r_{\text{max}} = 1.5\sigma$, and $\epsilon = 1$, where all energies are measured

in units of the thermal energy $k_B T$, and distances are measured in units of σ . Analogous repulsive 6-12 Lennard-Jones potentials parameterise the chain-crowder, chain-wall, and crowder-wall contact interactions. Along the axial z coordinate in our cylindrical geometry a harmonic potential is applied once a monomer attempts to move outside of the cylinder at $z < z_0 = 0$ or $z > z_L = L$. For both the crowding particles and the chain monomers we parametrized this potential as $U_z = k_z (z - z_0)^2 / 2$, with $k_z = 100$, and analogously for z_L .

The dynamics of the position $\mathbf{r}_i(t)$ of the i th monomer in a polymer chain is described by the Langevin equation

$$\begin{aligned} m \frac{d^2 \mathbf{r}_i(t)}{dt^2} = & - \sum_{j=1, j \neq i}^n \nabla U_{\text{LJ}}(|\mathbf{r}_i - \mathbf{r}_j|) - \nabla U_{\text{FENE}}(|\mathbf{r}_i - \mathbf{r}_{i \pm 1}|) \\ & - \sum_{j=1}^{N_{cr}} \nabla U_{\text{LJ}}(|\mathbf{r}_i - \mathbf{r}_{cr,j}|) - \nabla U_{\text{LJ}}(|\mathbf{r}_i - \mathbf{R}_{\text{cyl}}|) \\ & - \xi \mathbf{v}_i(t) + \mathbf{F}(t). \end{aligned} \quad (3)$$

Here m is the monomer mass, ξ is the friction coefficient, \mathbf{v}_i is the monomer velocity, and $\mathbf{F}(t)$ represents Gaussian noise with δ -correlations $\langle \mathbf{F}(t) \mathbf{F}(t') \rangle = 6k_B T \xi \delta(t - t')$. The standard Langevin thermostat is used. Similar Langevin equations are used for the dynamics of the positions $\mathbf{r}_{cr,j}$ of the crowding molecules in the presence of the confining cylinder at \mathbf{R}_{cyl} . Similarly to the procedure described in [67], we implement the velocity Verlet algorithm with the integration time-step of $\delta t = 0.01$. We use underdamped Langevin Dynamics with friction coefficient $\xi = 0.1$ and model the solvent implicitly.

The monomer size is set to $\sigma = 4$ nm, determining the chain thickness that stays constant for the different ring lengths simulated below. This thickness represents the effective physical DNA diameter including hydration water shells and electrostatic effects [68]. Our approach thus differs from that taken in [53], where the mixing of ring polymers of different lengths without a crowding agent was studied and the polymers were assumed to become thinner as they get longer. This assumption was used in [53] to keep a constant volume fraction ϕ_p of the polymer chains V_p in the simulation box of volume V , and it is estimated that [53]

$$\phi_p = \frac{\text{DNA volume}}{E. \text{ Coli volume}} = \frac{V_p}{V} \sim 1 \dots 5\%, \quad (4)$$

depending on the DNA thickness (the bare DNA diameter plus the electrostatic repulsive salt-dependent shell around it). We present the ring-ring contact number and overlap distance of rings for fixed ϕ_p using expanding simulation cells in figure 13, which represents the central result of our study.

The equilibration time of the polymer rings in our simulations depends on their length, the cell cylinder radius R , and the volume fraction ϕ of crowding particles in the simulation box. For typical parameters of the ring length

$$l = n\sigma \sim 200\sigma \quad (5)$$

and $R = 4.5\sigma$ used in the simulations below, the chains equilibrate after $\sim 4 \times 10^6$ simulation steps, corresponding to about 1 ms in real time, in the absence of crowders. The ring

equilibration time grows with the chain length, and longer measurement times are required in order to sample the conformations of the polymer chains. The equilibration time also grows with the volume fraction ϕ of crowders due to the slow-down of the polymer dynamics, see figure 9. More details on the equilibration procedure are presented in appendix A.

2.2. Crowding and confinement

We distinguish two types of volume confinement for the polymer chains: external confinement by the cylindrical cell walls and internal confinement by mobile crowding obstacles. The model cell in the majority of our simulations is represented by an impenetrable cylinder of length $L = 35\sigma$ and radius $R = 3.5\sigma \dots 5.5\sigma$.

By the internal confinement we mimic the poly-disperse soup of various proteins, RNA, cytoskeletal elements, and organelles in the cell cytoplasm. The crowders in the bacterial cytoplasm have an average molecular weight of $MW \approx 40 \dots 67$ kDa and diameter of 4...8 nm [59]. We neglect here the poly-dispersity in crowder sizes observed in real cells [69] and for simplicity assign to the crowders the same size $\sigma_{cr} = \sigma$ as for the chain monomers. The crowders are simulated as spherical particles of unit mass (similarly to the polymer bead), with systematically varying volume occupancy ϕ . Each polymer monomer therefore corresponds to ≈ 12 base pairs of the double-stranded DNA and $MW \approx 12 \times 0.66$ kDa. The characteristic time in our simulations then corresponds to a real time of $\tau_0 = \sigma \sqrt{12 \times 660 \text{Da} / (k_B T)} \approx 0.23$ ns. Simulating the crowders as particles with the more realistic value of MW of 67 kDa will slow down the crowder and polymer dynamics, renormalizing the elementary simulation time unit to $\tau_0 \approx 0.66$ ns.

Varying the volume fraction of crowders in the simulations in the range $0 < \phi \lesssim 0.3$ we mimic the response of a cell to the changes in external osmolarity, exerting a pressure on the outer cell membrane causing dehydration (osmotic upshift) [70]. This volume fraction is computed per free solution volume, i.e.,

$$\phi = \frac{V_{cr}}{V - V_p} = \frac{N_{cr}v}{\pi R^2 L - 2nv}, \quad (6)$$

where $v = 4\pi(\sigma/2)^3/3$ is the volume of one chain monomer or of one crowding particle and N_{cr} is the number of crowding particles in the box. For chain length $n = 200$ and cell length $L = 35\sigma$ the volume fraction of the two polymer rings is $\phi_p \approx 0.155, 0.094,$ and 0.063 (close to the DNA crowding in *E.coli* [53]) for the respective cylinder radii $R = 3.5\sigma, 4.5\sigma,$ and 5.5σ .

We consider only excluded volume interactions according to the above-mentioned interaction potentials and neglect other interactions within the ring polymers, including electrostatic interactions. The latter can be of importance for tightly bent and circular DNAs, particularly at low-salt, weak-screening conditions [71–73]. Our model also neglects hydrodynamic interactions (both for rings and crowders) [74, 75], which can alter the short-time polymer dynamics [76] but should not affect the static overlap properties of the rings. Polymer relaxation under confinement with and without hydrodynamic interactions was studied by computer simulations in [77]. For the relaxation time τ_R of a polymer ring consisting of n monomers in a long cylindrical pore of radius R the relation $\tau_R \sim n^2 R^{0.9}$ was predicted [44, 77].

2.3. Ring contacts and decay of correlations

For each simulation step t we determine the number of contacts $N_{AB}(t)$ between the two ring polymers as follows. Each monomer is surrounded by a sphere with contact radius $r_c = 1.25 \dots 2\sigma$ that defines the overlap volume. If the centers of mass of a monomer of another chain stays within this contact sphere for the contact time t_c , the contact is recorded as established. We chose $t_c = \tau_0$, but the results for the contacts are fairly insensitive to reasonable variations of t_c . The time t_c is a measure of the internal dynamics of two intermingled rings. Within this time scale, the change in distances between contacting monomers should be smaller than r_c . This validates the choice of the temporal and spacial thresholds for counting the number N_{AB} of ring-ring contacts.

The distance r_c represents the ‘radius of action’ within which the monomers are supposed to be involved in some physical interactions. For the DNA, this can be electrostatic or protein-mediated inter-molecular contacts [78]. Clearly, the results of counting the number N_{AB} of contacts depends on the threshold distance r_c (for comparison, the choice of $r_c = 1.5\sigma$ was used in [53]). We analyze the dependence of the contact number on the contact distance r_c in figure 11 below.

The average $\langle N_{AB} \rangle$ is computed via averaging over various polymer configurations after the system has reached its equilibrium. We measure the ring-ring overlap statistics after a sufficiently long equilibration time, $t > 10\tau_c(\phi)$, to ensure the decay of initial correlations of the polymers. Here τ_c is the correlation time for ring-ring contacts obtained from an exponential fit to the ring-ring overlap autocorrelation function defined below. In addition to the three-dimensional inter-chain contact probability, scaling with $\langle N_{AB} \rangle$, we compute the one-dimensional mutual overlap length of two rings along the z -axis of the confining cylinder, $\langle l_{AB} \rangle$. Note that we consider only torsionally relaxed rings, with no effects of super-coiling. The latter would result in more branched and topologically complex polymer structures, likely with more extensive contacts.

Following [53], we define the auto-correlation function (ACF) of ring-ring contacts via the contact number as follows

$$\text{ACF}(\Delta) = \frac{\langle N_{AB}(t + \Delta)N_{AB}(t) \rangle - \langle N_{AB}(t + \Delta) \rangle \langle N_{AB}(t) \rangle}{\langle N_{AB}(t)^2 \rangle - \langle N_{AB}(t) \rangle^2}. \quad (7)$$

The averaging $\langle \dots \rangle$ is performed over the times t along the generated trace $N_{AB}(t)$ with the corresponding lag time Δ . The ACF characterizes the decay of correlations in the overlap number of rings.

An additional quantity characterizing the ring-ring overlap is the relative position of their centers of mass,

$$\Delta z_{CM} = z_{CM,A} - z_{CM,B}. \quad (8)$$

From the corresponding probability density $p_{AB}(\Delta z_{CM})$ along the cylinder axis we compute the free energy of the overlap of the two rings in terms of

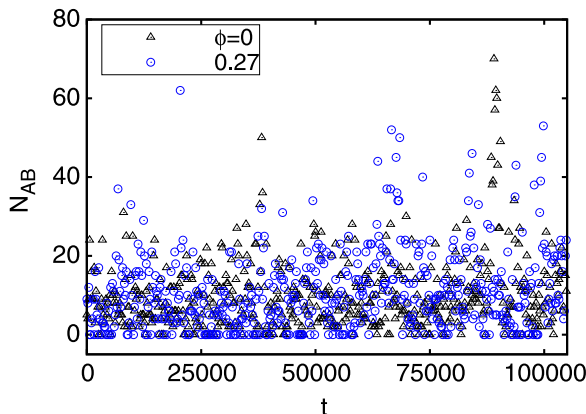


Figure 2. Fluctuations of the contact number $N_{AB}(t)$ of polymer rings as function of simulation time t , plotted for crowding fractions $\phi = 0$ and 0.27 . Parameters: the number of monomers in each ring is $n = 200$, the radius of the confining cylinder is $R = 4.5\sigma$, the critical contact distance is $r_c = 1.5\sigma$, and the cylinder length is $L = 35\sigma$. Here and below the simulation time is presented in units of the characteristic time τ_0 .

$$F(z_{CM}) = -k_B T \ln [p_{AB}(z_{CM})] \quad (9)$$

in the Shannon sense.

3. Results

3.1. Dimensions and contacts of polymer rings

We verified that the extension of an unconfined ring polymer scales with its length as

$$\langle R_g^2(n) \rangle \sim n^{2\nu}, \quad (10)$$

where $\nu = 3/5$, consistent with the results reported in [57] (not shown). Our polymer rings are very flexible, the effective persistence length l_p being of the order of the monomer size (data not shown). Because of this extreme chain flexibility, we cannot analyze the implications of confinement onto the chain persistence (as compared to [44] where ring polymers were shown to stiffen substantially in tight confinement). Under the cylindrical confinement, the ring size $\langle R_g^2 \rangle$ naturally reaches a saturation for long chains. Once the chain dimensions overcome the size of the cylindrical cell, the polymer starts to fold on itself and its apparent scaling exponent ν decreases.

The initial ring configurations at $t = 0$ generated in the simulations are well separated, positioned at the opposite sides of the confining cylinder. They exhibit a fast initial relaxation followed by a roughly exponential relaxation dynamics. At the later stages, when the polymers experience external confinement by the cylinder and the other ring, a non-exponential relaxation dynamics sets in. The spectrum of chain fluctuations in frequency space in the presence of external confinement and crowding becomes altered as well.

The general trend is that the instantaneous number of ring-ring contacts $N_{AB}(t)$ fluctuates strongly in the course of the simulations; compare figure 2. This trend is the same as in recent simulations for a similar system presented in the supplementary material of [53]. We observe

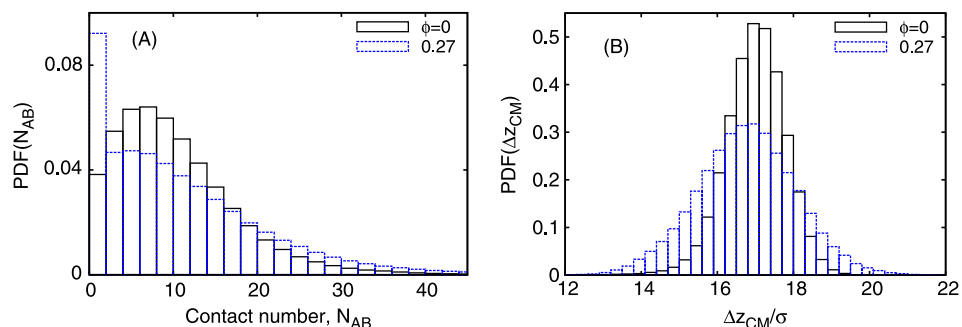


Figure 3. Probability density function of the ring-ring contact number (A) and centers of mass difference of the two rings (B), plotted for the parameters of figure 2.

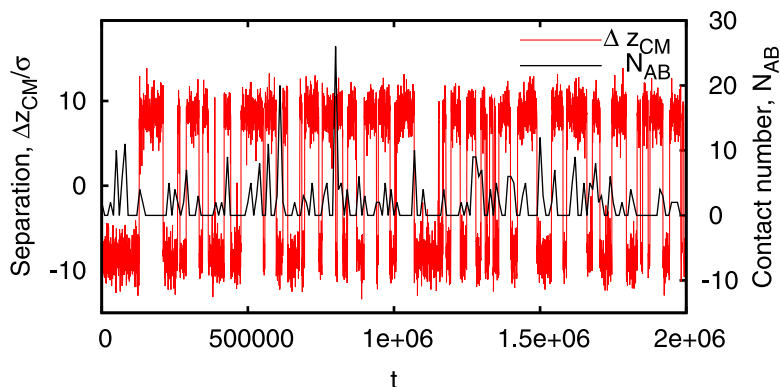


Figure 4. Time traces for the contact number $N_{AB}(t)$ (black) and the center of mass relative distance of the rings Δz_{CM} (red). Every 10,000th and 400th data point is shown for the $N_{AB}(t)$ and $\Delta z_{CM}(t)$ trajectories, respectively. Parameters: no crowders ($\phi = 0$), chain length $n = 60$, cylinder radius $R = 5.5\sigma$, and length $L = 20\sigma$. A video illustrating the ring swapping events is included in the online supplementary material (available at stacks.iop.org/njp/16/053047/mmedia).

that in the presence of crowders the ring-ring separation becomes more pronounced, and the probability density function $\text{PDF}(N_{AB})$ of their contact numbers exhibits a peak at $\langle N_{AB} \rangle = 0$. The spread of N_{AB} is slightly more localized in the presence of crowders, but at both crowded and non-crowded conditions the distributions $p(N_{AB})$ have long tails, as evidenced in figure 3 (A). The relative center-of-mass position of the two rings, Δz_{CM} , shows a larger spread in the presence of crowders; see figure 3(B).

3.2. Ring swapping

For some choices of the volume and the aspect ratio of the confining cylinder as well as for shorter polymer lengths, the directed distance Δz_{CM} between the centers of mass of the two ring polymers exhibits clear alternations between two states while the rings are well separated near the ends of the confining cylinder; see figure 4. For such conditions, the diffusion times of the rings along the cylinder are relatively short, so they can pass one another and swap positions. At

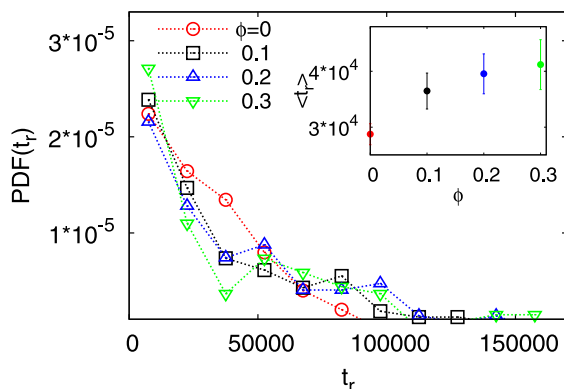


Figure 5. Normalized distribution of residence times t_r in the well-segregated ring states. The histograms are obtained from the zigzag traces similar to those presented in figure 4, but at varying crowding fractions. The inset shows the mean residence time of rings $\langle t_r \rangle$ in well-separated states as a function of ϕ .

time instances when the rings are well separated the number of ring-ring contacts is minimal, while at almost vanishing center of mass separation, $z_{CM} \sim 0$, the overlap of the rings is maximal and thus typically the $N_{AB}(t)$ traces are peaking at these instances; see the time series of $\Delta z_{CM}(t)$ and $N_{AB}(t)$ shown in figure 4. Note that the center of mass distance $|\Delta z_{CM}| \leq L$, and the case of $\Delta z_{CM} > 0$ corresponds to the situation in which ring A is located on the left half and ring B on the right half of the confining cylinder. This type of dynamics is reminiscent of the periodic tumbling of polymers in shear flows, characterized by configurations with large extensions alternating with states of strong chain contraction; see, e.g., the studies reported in [79, 80].

For these conditions of well-separated rings, the distribution of residence times t_r , such that each ring is situated in one of the two well-separated states close to the cylinder ends, is shown in figure 5 for different ϕ . The mean residence time $\langle t_r \rangle$ extracted from these histogram is the characteristic time scale for the internal ring swapping dynamics. As shown in the inset of figure 5, $\langle t_r \rangle$ mildly increases with increasing ϕ . The maximum of the residence time histograms in figure 5 shifts at higher crowding fractions to larger values because of the associated slower polymer dynamics.

As illustrated in figure 6 the effective free energy for swapping the two rings has a double-well shape. The height of the barrier separating the two minimum states amounts to several $k_B T$ for the parameters used in the simulations. As the residence times t_r in these separated ring states increases, the height of the free energy barrier between them decreases. This is due to the slower polymer dynamics at high crowding fractions, as discussed below. It also demonstrates that the free energy landscape is no true equilibrium measure, as known from the theory of polymer translocation [80]. The dynamics of ring swapping in more crowded solutions is overwhelmed by the enhanced viscosity, as compared to the effects of reduced free energy barriers. For instance, we found that the effective viscosity for the diffusion of a single crowder rises about 4 times as ϕ changes from 0 to 0.3 [65]. Longer rings squeezed into the same confining cylinder reveal a slower swapping dynamics and the residence times in well-separated states grow until

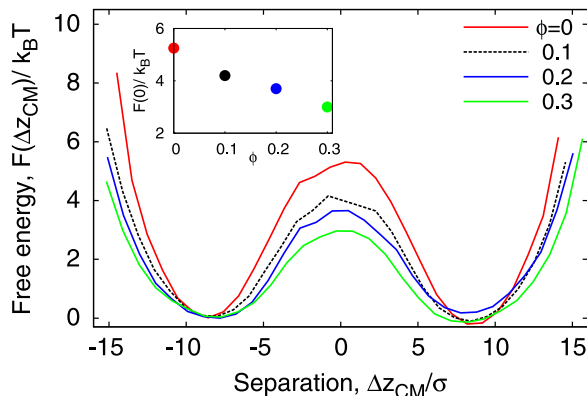


Figure 6. Double-well free energy landscape for ring swapping. The inset shows the magnitude of the free energy barrier computed at $\Delta z_{CM} = 0$. Parameters and notations for the curves are the same as in figure 5.

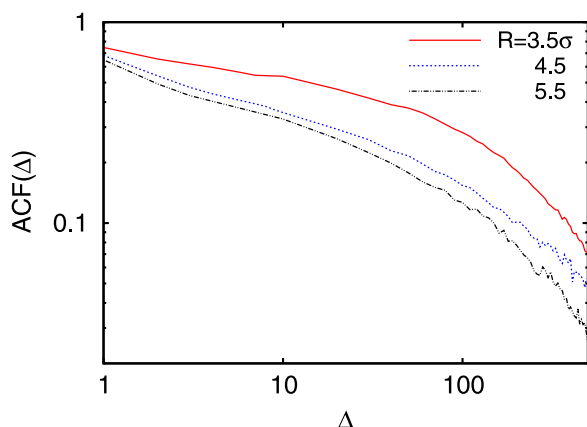


Figure 7. ACF of the ring-ring contact number N_{AB} defined in equation (7) in absence of crowders ($\phi = 0$) for different values R of the cylinder radius. Other parameters are the same as in figure 2.

no swapping at all can be observed during the simulation time. Likewise, the exchange of rings in the simulation box is prohibited for smaller cylinder radii R , as we examine for the range of parameters in the subsequent sections.

3.3. Correlations of ring-ring contacts

As demonstrated in figure 2, the number of ring-ring contacts fluctuates strongly and irregularly. To find a typical time-scale for this variation, we compute the ACF (7) of the ring-ring contact number from the $N_{AB}(t)$ time traces. We start with the crowding-free case $\phi = 0$. The resulting curves in figure 7 show a fast relaxation at short times and turn to a nearly exponential decay at intermediate lag times Δ . At long times, the ACF drops to zero, indicating a complete loss of correlations. Some fluctuations of the ACF(Δ) at $\Delta \rightarrow \infty$ indicate insufficient statistics in the calculation of the time average (7). From figure 7, we observe that the initial decay of the ACF is slower for smaller cylinder radii, as expected. This is due to a

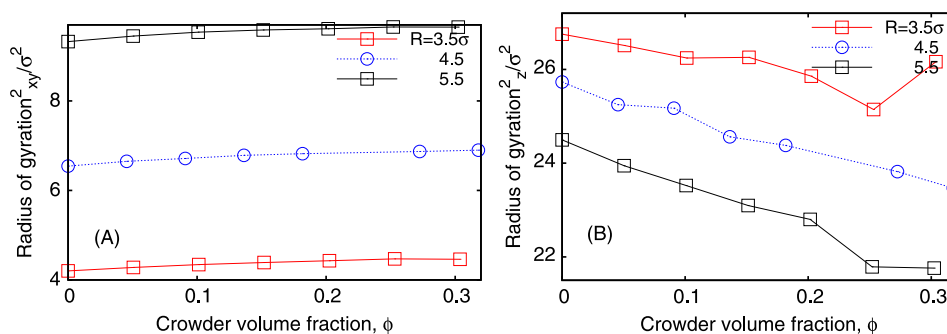


Figure 8. Mean squared gyration radius $\langle R_g^2 \rangle$ of a single polymer ring in the system of two mixing rings across the confining cylinder (A) and along the cylinder axis (B), computed for varying crowding fractions ϕ and different radii R of the cylinder. Other parameters are the same as in figure 2.

larger space fraction in the simulation box being filled by the polymer monomers so that their motions get restricted to a larger extent, with many chains' moves being prohibited. For longer rings confined in the same cylinder, the ACF decays more slowly with the lag time Δ , again due to a smaller space available for the chains (not shown). Note that the intermediate-time decay exhibits comparable slopes in the logarithmic plot of figure 7.

3.4. Contacts and overlap of polymer rings: crowding effects

Let us now study the effects of the internal confinement due to crowding in more detail. We first consider one of the two ring polymers under the cylindrical confinement in the presence of crowding agents. The results for the mean squared gyration radius $\langle R_g^2 \rangle$ are shown in figure 8. We observe that the component of the radius of gyration measured along the cylinder axis is a slowly decreasing function of ϕ . Crowding particles thus act as a depletant, which effects ring shrinkage. For a less severe external confinement (larger cylinder radius R), we observe that the ring is less extended along the cylinder axis, but simultaneously more extended in the cylinder cross-section ($x - y$ plane), as shown in figure 8(A). Here we do not elaborate on the variation of the Flory scaling exponent ν of the gyration radius for a single ring as function of the external confinement and crowding (for such results see, e.g., those reported in [59]). In the following we concentrate on the overlap properties of two polymer rings in the cylindrical simulations cell.

At higher fractions ϕ of crowders the correlation time of maintaining the established contacts between polymer rings increases due to the slower polymer dynamics, following a larger effective viscosity in a denser soup of crowders, i.e., the Rouse polymer dynamics is effectively slowed down by surrounding crowding particles. Concurrently, the same effect is responsible for a slower decay of the contact autocorrelations at higher values of ϕ , as shown in figure 9. The associated correlation time τ_c extracted from an exponential fit of the ACF(Δ) curves exhibits the power-law dependence

$$\tau_c(\phi) \sim \phi^{3/2} \quad (11)$$

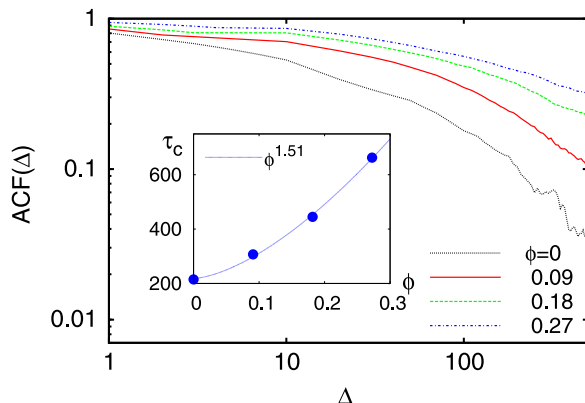


Figure 9. ACF function of ring-ring contacts, equation (7), for different crowding fractions ϕ and the parameters of figure 2. The inset shows the correlation time $\tau_c(\phi)$ determined from the decay $\exp(-\Delta/\tau_c)$ of the ACF(Δ) curves.

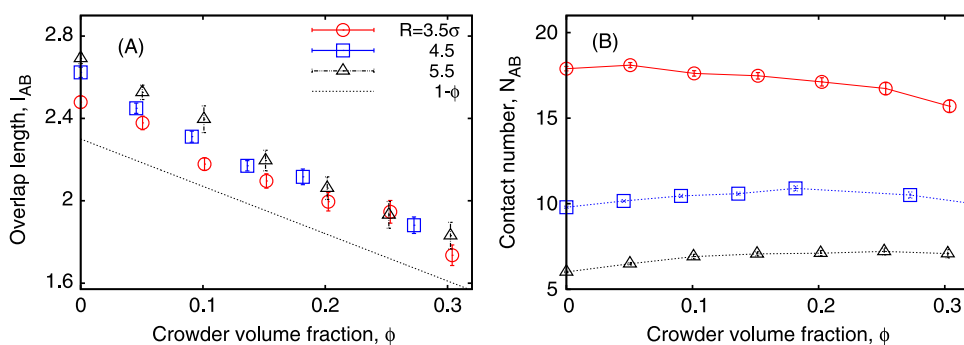


Figure 10. Average ring-ring overlap length along the cylinder axis (A) and average contact number (B), plotted for $L = 35\sigma$. The $(1 - \phi)$ asymptote in panel (A) represents the proportionality to $(1 - \phi)$ given by equation (12).

on the fraction of crowders; see the inset of figure 9. The $3/2$ exponent indicates that the changes due to crowding are indeed a volume effect. Note that the single-ring relaxation time τ_R should not be confused with τ_c for the ring-ring contacts.

The dependence on the presence of mobile crowders of the three-dimensional contact characteristics and the effective one-dimensional overlap properties of polymer rings of fixed length are analyzed in figure 10. We observe that the average number of ring-ring contacts $\langle N_{AB} \rangle$ increases significantly with the decrease of the cylinder radius R , i.e., when the chains are forced into a stronger contact by the external confinement; see figure 10(B). As function of the internal confinement due to crowding, in some situations the number of ring-ring contacts N_{AB} exhibits a weakly non-monotonic dependence; see, e.g., the blue symbols in figure 10(B). This behavior indicates a tradeoff between crowding and external confinement.

The effective overlap length of the rings along the cylinder axis is, in contrast, a very reproducible function with the functional relation

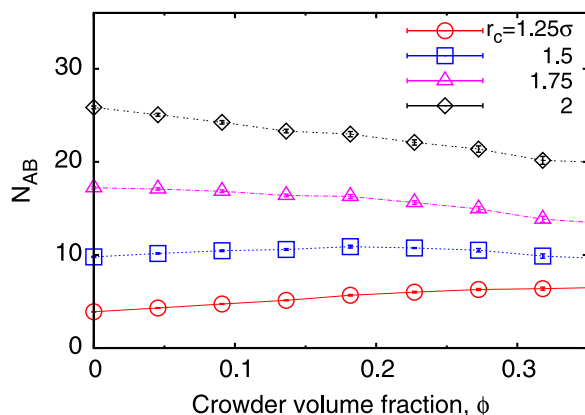


Figure 11. Average number of ring-ring contacts computed for varying contact radius r_c at cylinder radius $R = 4.5\sigma$. Other parameters are the same as in figure 10.

$$\langle l_{AB}(\phi) \rangle \approx \langle l_{AB}(0) \rangle (1 - \phi). \quad (12)$$

of the crowding fraction ϕ , compare figure 10A. This fact indicates a nearly ideal mixing of polymer monomers and crowding particles, as if the chain connectivity plays a minor role. The absolute values of l_{AB} for different cylinder radii vary only marginally. The decrease in equation (12) can be understood from a shrinkage of individual ring polymers by the crowders, as rationalized for longitudinal ring dimensions in figure 8(B). We note a relatively short overlap length at all crowding densities used in the simulations. It is also consistent with the results of [53] where, in the absence of crowders, a very limited inter-penetration and overlap of the two polymer rings was obtained.

We also systematically examined the effect of the contact radius r_c on the number of ring-ring contacts established in the simulations. We find that the average number of contacts naturally grows with r_c ; compare figure 11. We also note that the error bars somewhat increase with ϕ and r_c but always stay smaller than the symbol size. Here and below, as proposed in [53], for the ring-ring contacts the error bars are computed with the blocking method introduced for correlated data sets in [82].

The statistical effects of the polymer-crowder mixing are analyzed in terms of their distributions in the simulation cell. We find that for weak and moderate crowding fractions there is an accumulation of crowders near the cylinder ends, as evidenced in figure 12(A). Following the trend of demixing, the polymer monomers are located preferentially off the middle of the cylinder; see figure 12(B). We also observe that at small ϕ the crowding particles are effectively excluded from regions occupied by the polymers, thus facilitating ring-ring contacts. At stronger crowding, a moderate peak of crowding particles in the middle of the cell (between the polymer rings) emerges; see the blue curve in figure 12(A). These mid-positioned crowding particles trigger an entropy-driven segregation of polymer rings, and their three-dimensional contact number N_{AB} decreases at larger ϕ values (figure 13(B)).

The mixing properties of polymers and crowders can be probed by the cumulative probability distribution of their monomers, shown figure 12(C). The decrease of $N_{AB}(\phi)$ at high ϕ is due both to a progressive emergence of crowders in between the polymers and a longitudinal shrinkage of each of the rings with ϕ . The ideal $(1 - \phi)$ polymer-crowder mixing

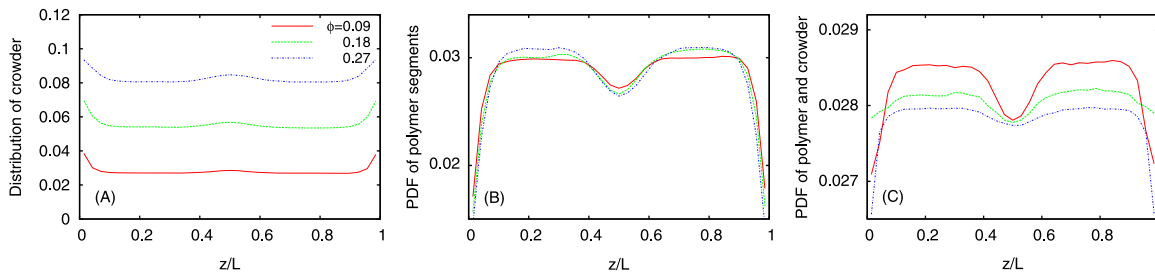


Figure 12. Distribution of crowding particles (A), polymer monomers (B), and the cumulative crowder-polymer distribution (C), plotted along the cylinder axis for varying ϕ fractions. Parameters are the same as in figure 2.

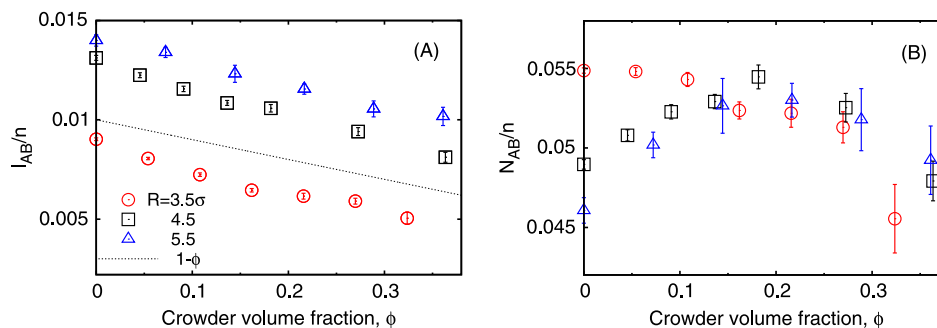


Figure 13. Relative overlap length (A) and contact number of polymer rings (B) in expanding simulation cells. In this figure the polymer volume fraction is kept constant at $\phi_p \approx 0.09$, and the length of the polymer rings is $n = 102, 200,$ and 348 monomers for cylinder radii of $R = 3.5\sigma, 4.5\sigma, 5.5\sigma$, respectively. Note the larger deviations around the mean for the contact numbers N_{AB} at more crowded conditions (the error bars are computed by the blocking method [83]). The square symbols represent the same data set as in figure 10(B) for $R = 4.5\sigma$. The $(1 - \phi)$ asymptote in panel (A) indicates the dependence on the value in the uncrowded solution, $l_{AB}(\phi = 0)$, as given by equation (12).

is realized at high ϕ , when the sum of the distributions of the polymer monomers and crowders is almost constant throughout the simulation cell; see the blue curve in figure 12(C).

3.5. Variation of the polymer length

In the previous sections, most of the results presented were obtained for a constant polymer length of $n = 200$ monomers and relatively small simulation cells. To be able to scale up our results to ranges relevant for bacteria cells, we computed the ring-ring overlap length and contact number for longer polymers and larger simulation cells. The geometrical proportions of the confining cylinder, the aspect ratio R/L , were kept constant and at the same time the ring length was adjusted so the polymer volume fraction $\phi_p = V_p/V$ stayed constant at $\phi_p \approx 0.09$. We observe that both the one-dimensional overlap length of the polymer rings and their three-dimensional contact number follow universal trends, after normalization with respect to the number of monomers, i.e., for l_{AB}/n and N_{AB}/n . These results are illustrated in figure 13, which is

the main result of this work. The ring-ring overlap length follows the $(1 - \phi)$ -asymptote typical for the ideal mixing for all the parameters analyzed in our simulations. In contrast, the number of contacts N_{AB} reveals a more delicate dependence. For small confining cylinders the contact number is a monotonically decreasing function (red symbols in figure 13(B)). For larger simulation cells, the value of $N_{AB}(\phi)$ exhibits a maximum at $\phi \approx 0.2$ (black and blue symbols in figure 13(B)). This fraction $\phi \approx 20\%$ is reminiscent of the turning-point value for the non-monotonic dependencies on the fraction of crowding molecules mentioned in the Introduction, namely, of the dimensions of self-avoiding polymers [58] and diffusion-limited chemical reactions [61].

To compute l_{AB}/n and N_{AB}/n , we averaged over $M = 2 \times 10^5$, 2×10^5 , and 8×10^4 simulation steps for cylinder radii $R = 3.5\sigma$, 4.5σ , 5.5σ , respectively. The simulation time on a standard 3–3.5 GHz core machine for each crowding fraction ϕ presented in figure 13 is about 2, 3, and 10 days, respectively. To accumulate reliable statistical information about the ring-ring contacts at relatively large crowding fractions, particularly long simulations are required because of the slower dynamics of inter-ring mixing. Last, at the same volume fraction of crowders ϕ , one can expect crowding particles of larger sizes to cause stronger effects on mixing properties of polymer rings.

4. Discussion and conclusions

Based on extensive Langevin dynamics simulations we analyzed the behavior of polymer chains of a circular topology in the presence of external cylindrical confinement and internal crowding by molecular crowding agents. The size of the cylindrical confinement with respect to the length of the chains was chosen to represent the situation of two DNA rings in a typical bacillus cell. The crowding agents were represented by thermally agitated, off-lattice mono-disperse hard spheres. Our main result, presented in figure 13, is that high concentrations of crowding agents facilitate the spatial separation of ring polymers in cylindrical confinement. In addition, we quantified the extent to which the presence of crowding agents slows down the dynamics of the polymer-crowder system. The simulations for chains of varying length demonstrate that our model results are robust and in principle scalable to the dimensions of real bacterial cells.

The effect of molecular crowding on crowding-mediated polymer separation obtained above are applicable to demixing and mutual exclusion of genome-sized DNA molecules inside bacterial cells⁴ as well as to the behavior of relatively short DNA plasmids confined in natural compartments inside eukaryotic cells. The abundance of macromolecular crowders also offers a robust and non-specific way to tune the amount of DNA-DNA contacts. The dynamics and spatial occurrence of the latter are vital for biological processes *in vivo* such as DNA-DNA recognition and DNA homologous recombination [53], when the search for the homologous DNA partner in a coil of a long DNA is to be performed. Note that it would be interesting to analyze how the DNA-crowder segregation takes place in bacteria with other than rod-like shapes, such as in nearly planar squarish or spherical bacteria; see the discussion in [37].

⁴ Recent experiments show that in *E. coli* active protein oscillations guide the demixing of the chromosomes and thus assist entropic effects, see [83].

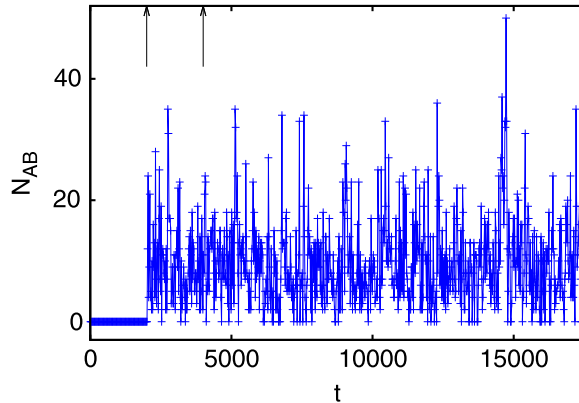


Figure A1. Contact number of two chains during a typical run including the initial equilibration interval. Initially the contacts are zero, as the chains are well separated. At the first arrow the confining cylinder's length is reduced to the actual value L intended for the simulations. The second arrow indicates when we start to record the time series of N_{AB} . The data correspond to a chain length of 200, cylinder radius $R = 4.5$, and cylinder length $L = 35$.

The compartmentalization of obstacles and polymer chains we observed in figure 12 can also have implications for aging phenomena of bacterial cells. For *E. coli* cells, for instance, a localization of age-related protein aggregates in low-crowding regions near the cell poles and in between the two DNA nucleoids was observed. This effect was recently quantified by computer simulations at higher degrees of polymer and DNA crowding inside the nucleoids that hinder the diffusion of these protein aggregates [84]. The impairment of the diffusion of aggregating components, which is a heterogeneous effect in a compartmentalized cell, thus directly affects the rate of aggregate formation.

Acknowledgments

JS thanks W K Kim for providing a computer code for analysis of ring swapping dynamics. The authors acknowledge funding from the Academy of Finland (FiDiPro scheme to RM), the Deutsche Forschungsgemeinschaft (DFG Grant CH 707/5-1 to AGC), and the German Federal Ministry for Education and Research (to JS).

Appendix A. Equilibration in the simulations

The chain equilibration in our simulations is performed as follows. Initially two chains are separated inside a confining cylinder, whose length is larger than the actual cylinder length L we intend to simulate. The length is then gradually decreased to the value L , while the chains are allowed to move. During this procedure we monitor the contact number N_{AB} , as shown in figure A1. As can be seen, the two chains are initially well separated and $N_{AB} = 0$. The first arrow indicates when the cylinder length shrinks to the value L . We then let the system evolve until the second arrow, from which we record the time series $N_{AB}(t)$. The time span between the two arrows corresponds to about 10 times the correlation time τ_C .

References

- [1] Jun S and Wright A 2010 *Nature Rev. Microbiol.* **8** 600
- [2] Hancock R 2012 *PLoS ONE* **7** e36045
- [3] Dekker J, Marti-Renom A and Mirny L A 2013 *Nature Rev. Genet.* **14** 390
- [4] Lee T B K *et al* 2013 *Science* **342** 731
- [5] Bates D and Kleckner N 2005 *Cell* **121** 899
- [6] Cremer T and Cremer C 2001 *Nature Rev. Genet.* **2** 292
- [7] Dorier J and Stasiak A 2009 *Nucl. Acids Res.* **37** 6316
- [8] Rosa A and Everaers R 2008 *PLoS Comput. Biol.* **4** e1000153
- [9] Rosa A, Becker N B and Everaers R 2010 *Biophys. J.* **98** 2410
- [10] Bronstein I, Israel Y, Kepten E, Mai S, Shav-Tal Y, Barkai E and Garini Y 2009 *Phys. Rev. Lett.* **103** 018102
- [11] Kroy K and Glaeser J 2007 *New J. Phys.* **9** 416
- [12] Marenduzzo D *et al* 2009 *Proc. Natl. Acad. Sci. USA* **106** 22269
- [13] Saper G *et al* 2013 *Nucl. Acids Res.* **41** 1569
- [14] Leforestier A, Siber A, Livolant F and Podgornik R 2011 *Biophys. J.* **100** 2209
- [15] Hanke A, Metzler R, Dommersnes P G, Kantor Y and Kardar M 2003 *Eur. Phys. J. E* **12** 347
- [16] Zhang C *et al* 2009 *Proc. Natl. Acad. Sci. USA* **106** 16651
- [17] Zimmerman S B and Murphy L D 1996 *FEBS Lett.* **390** 245
- [18] McGuffee A R and Elcock A H 2010 *PLoS Comp. Biol.* **6** e1000694
- [19] Zimmerman S B and Minton A P 1993 *Annu. Rev. Biophys. Biomol. Struct.* **22** 27
- [20] Yanagisawa M, Sakaue T and Yoshikawa K 2014 *Intl. Rev. Cell & Molec. Biol.* **307** 175
- [21] Denton A R 2014 *Intl. Rev. Cell & Molec. Biol.* **307** 27
- [22] Weiss M 2014 *Intl. Rev. Cell & Molec. Biol.* **307** 383
- [23] Goychuk I 2012 *Adv. Chem. Phys.* **150** 187
- [24] Jeon J-H, Martinez-Seara Monne H, Javanainen M and Metzler R 2012 *Phys. Rev. Lett.* **109** 188103
Jeon J-H, Leijnse N, Oddershede L and Metzler R 2013 *New J. Phys.* **15** 045011
- [25] Guigas G, Kalla C and Weiss M 2007 *Biophys. J.* **93** 316
- [26] Barkai E, Garini Y and Metzler R 2012 *Phys. Today* **65** 29
Höfling F and Franosch T 2013 *Rep. Prog. Phys.* **76** 046602
- [27] Golding I and Cox E C 2006 *Phys. Rev. Lett.* **96** 098102
- [28] Weber S C, Spakowitz A J and Theriot J A 2010 *Phys. Rev. Lett.* **104** 238102
- [29] Szymanski J and Weiss M 2009 *Phys. Rev. Lett.* **103** 038102
- [30] Jeon J-H, Tejedor V, Burov S, Barkai E, Selhuber-Unkel C, Berg-Sørensen K, Oddershede L and Metzler R 2012 *Phys. Rev. Lett.* **106** 048103
- [31] Tabei S M A, Burov S, Kim H Y, Kuznetsov A, Huynh T, Jureller J, Philipson L H, Dinner A R and Scherer N F 2013 *Proc. Natl. Acad. Sci. USA* **110** 4911
- [32] Zhou H X 2004 *J. Mol. Recognit.* **17** 368
- [33] Echeverria C and Kapral R 2012 *Phys. Chem. Chem. Phys.* **14** 6755
- [34] Brackley C A, Cates M E and Marenduzzo D 2013 *Phys. Rev. Lett.* **111** 108101
- [35] Stiehl O, Weidner-Hertrampf K and Weiss M 2013 *New J. Phys.* **15** 113010
- [36] Kühn T *et al* 2011 *PLoS One* **6** e22962
- [37] Jun S 2010 Polymer physics for understanding bacterial chromosomes *Bacterial Chromatin* ed R T Dame and C J Dorman (Berlin: Springer) chapter 6 pp 97–116
- [38] Jun S and Mulder B 2006 *Proc. Natl. Acad. Sci. USA* **103** 12388
- [39] Metzler R, Kantor Y and Kardar M 2002 *Phys. Rev. E* **66** 022102
- [40] Rubinstein M 1986 *Phys. Rev. Lett.* **57** 3023
- [41] Micheletti C and Orlandini E 2012 *Macromol.* **45** 2113
- [42] Tubiana L *et al* 2011 *Phys. Rev. Lett.* **107** 188302

- [43] Micheletti C, Marenduzzo D and Orlandini E 2011 *Phys. Rep.* **504** 1
- [44] Jung Y *et al* 2012 *Soft Matter* **8** 2095
- [45] Benedetti F, Dorier J, Burnier Y and Stasiak A 2014 *Nucl. Acids Res.* **42** 2848
- [46] Narros A *et al* 2013 *Macromol.* **46** 3654
- [47] Reigh S Y and Yoon D Y 2013 *ACS Macro Lett.* **2** 296
- [48] Kim J *et al* 2013 *Soft Matter* **9** 6142
- [49] Mateos-Langerak J *et al* 2009 *Proc. Natl. Acad. Sci. USA* **106** 3812
- [50] Bohn M and Heermann D W 2010 *J. Chem. Phys.* **132** 044904
Bohn M *et al* 2010 *Macromol.* **43** 2564
- [51] Fritsche M and Heermann D W 2012 *Soft Matter* **7** 6906
- [52] Racko D and Cifra P 2013 *J. Chem. Phys.* **138** 184904
- [53] Dorier J and Stasiak A 2013 *Nucl. Acids Res.* **41** 6808
- [54] Halverson J D *et al* 2014 *Rep. Prog. Phys.* **77** 022601
- [55] Reisner W, Pedersen J N and Austin R H 2012 *Rep. Prog. Phys.* **75** 106601
- [56] Micheletti D *et al* 2014 *ACS Macro Lett.* **3** 255
- [57] Orlandini E *et al* 2010 *Phys. Rev. E* **82** 050804(R)
- [58] Parisi G and Sourlas N 1981 *Phys. Rev. Lett.* **46** 871
- [59] Kim J S *et al* 2011 *Phys. Rev. Lett.* **106** 168102
- [60] Kim J S and Szleifer I 2010 *J. Phys. Chem. C* **114** 20864
- [61] Schmit J D, Kamber E and Kondev J 2009 *Phys. Rev. Lett.* **102** 218302
- [62] Marcovitz A and Levy Y 2013 *Biophys. J.* **104** 2042
- [63] Gopinathan A and Kim Y W 2007 *Phys. Rev. Lett.* **99** 228106
- [64] Chen Y and Luo K 2013 *J. Chem. Phys.* **138** 204903
- [65] Lappala A, Zaccane A and Terentjev E M 2013 *Scientific Reports* **3** 3103
- [66] Shin J, Cherstvy A G and Metzler R 2014 in preparation
- [67] Shin J, Cherstvy A G and Metzler R 2014 *Phys. Rev. X* **4** 021002
- [68] Rybenkov V V, Vologodskii A V and Cozzarelli N R 1997 *Nucl. Acids Res.* **25** 1412
- [69] McGuffee A R and Elcock A H 2013 *PLoS Comp. Biol.* **6** e1000694
- [70] Mika J T 2010 *et al Mol. Microbiol.* **77** 200
- [71] Savelyev A, Materese C K and Papoian G A 2011 *J. Am. Chem. Soc.* **133** 19290
- [72] Cherstvy A G 2011 *J. Biol. Phys.* **37** 227
- [73] Cherstvy A G 2011 *J. Phys. Chem. B* **115** 4286
- [74] Ando T and Skolnick J 2010 *Proc. Natl. Acad. Sci. USA* **107** 18457
- [75] Wensink H H *et al* 2012 *Proc. Natl. Acad. Sci. USA* **109** 14308
- [76] Hegde G A *et al* 2011 *J. Chem. Phys.* **135** 184901
- [77] Jung Y *et al* 2009 *Phys. Rev. E* **79** 061912
- [78] Cherstvy A G and Teif V B 2013 *J. Biol. Phys.* **39** 363
- [79] Winkler R G 2006 *Phys. Rev. Lett.* **97** 128301
- [80] Huang C C *et al* 2012 *J. Phys.: Cond. Matt.* **24** 284131
- [81] Chuang J, Kantor Y and Kardar M 2001 *Phys. Rev. E* **65** 011802
Luo K, Ala-Nissila T, Ying S-C and Metzler R 2009 *Europhys. Lett.* **88** 68006
- [82] Flyvbjerg H and Petersen H G 1989 *J. Chem. Phys.* **91** 461
- [83] di Ventura B *et al* 2013 *Mol. Systems Biol.* **9** 686
- [84] Coquel A S *et al* 2013 *PLoS Comput. Biol.* **9** e1003038